1984

Polyurethane-Urea Elastomers as Working Substances in Rubber Heat Engines

William MacKnight, *University of Massachusetts Amherst*
R. E. Lyon
D. X. Wang
R. J. Farris

Polyurethane–Urea Elastomers as Working Substances in Rubber Heat Engines

R. E. LYON, D. X. WANG, R. J. FARRIS, and W. J. MacKNIGHT,
*Department of Polymer Science and Engineering, University of
Massachusetts, Amherst, Massachusetts 01003*

Synopsis

The possibility of using synthetic elastomers as working substances in a rubber heat engine
was investigated at the laboratory and pilot scale. Two polyurethane–urea elastomers were
subjected to experimental heat engine cycles at a variety of strains and temperature differences. It was found that optimum power and thermal efficiency were obtained at small strain
perturbations where the elastomers were close to mechanical equilibrium. Crystallization of
the rubbery phase during large strain perturbations is a nonequilibrium process which should
be avoided. Quasi-ideal rubber behavior is approached in the pilot-scale heat engine which
supports these conclusions.

INTRODUCTION

The conversion of heat energy into mechanical energy in a closed cycle
engine is accomplished by formulating a mechanism by which the working
substance is made to undergo a series of thermodynamic processes and
ultimately return to the initial state. The energy balance for such a cycle
is given by the first law of thermodynamics, which is completely general
and imposes no restrictions on the nature of the working substance. Indeed,
any substance (gas, liquid, or solid) may be used provided it is able to undergo
a reversible cyclic process.

By far the most common working substances in heat engine cycles are
gas vapor and vapor–liquid mixtures. This is due to the high performance
of these substances in engines utilizing large heat fluxes as may be obtained
from fossil and nuclear fuels. However, a growing awareness of the finite
supply of these energy sources has stimulated considerable interest in developing heat engines which can utilize waste heat and renewable energy
sources such as solar, geothermal, and ocean thermal. The small temperature differentials associated with these heat sources preclude the use of
most conventional gas or vapor–liquid cycles. This is because adverse factors
such as adiabatic heating of the gas and temperature drops through containment walls and boundary layers become prohibitive at the level of waste
heat and environmental temperatures.

For this reason, heat engines have been proposed utilizing solids as the
working substance, since these materials can interact directly with the
thermal source to extract heat. Materials which have been used in solid-state heat engines include a metal alloy,[1] rubbery polymers,[2-5] and crys-

CCC 0021-8995/84/092857-16$04.00

talline polymers.[6,7] Rubbery polymers have also functioned in reversed cycles as heat pumps.[8]

In addition to converting heat into work in these thermomechanical cycles, polymers have been synthesized which can convert chemical energy[9-11] and electromagnetic energy[12,13] into useful work as well. The specific mechanism by which polymers interact with these diverse energy sources to do work depends on the physical and chemical structure of the individual polymer material. However, it is the ability of polymers and gases alike to store and release mechanical energy as changes of entropy, which provides the thermodynamic route to power production using these materials.[14,15]

The purpose of this paper is to examine the thermodynamic behavior of two synthetic polyurethane–urea elastomers subjected to experimental (Stirling) heat engine cycles. This study follows from a previous analysis of the suitability of ideal elastomers for heat engine cycles,[5] in an attempt to explain the actual performance of a pilot-scale rubber heat engine for which some data is also presented. The elastomers investigated have functioned as working substances in this rubber heat engine and achieved power densities of 1 kW/kg elastomer.[16]

Experiments were conducted in which the elastomers were cycled in a quasiequilibrium manner through a thermomechanical cycle in an effort to reproduce the operating cycle of the rubber heat engine. These "power cycles" were obtained over a wide range of strains and temperatures in order to determine conditions for optimum performance and are compared with pilot-scale engine data. The observed nonideal behavior of these elastomers is attributed primarily to the strain-induced crystallization and melting occuring during loading and unloading. This is analagous to the condensation–vaporization phase change of a gas and has similar consequences with regard to heat engine performance.

MATERIALS

The two elastomeric fibers used in this study are commercially available coalesced multifilament yarns whose chemistry, properties, and manufacture have been described.[17,18] Chemically these fibers are linear block copolymers composed of approximately 15 wt % hard segment and 85 wt % soft segment. The terms "hard" and "soft" refer to polymer chain segments below and above their glass transitions, respectively.

The hard segment blocks of both fibers are the same, being composed of 4,4′-diphenylmethane diisocyanate (MDI) with ethylene diamine as the chain extender. These hard segments are crystalline in the pure state and melt at approximately 210°C as they exist in the fiber.

The soft segments of these elastomer fibers are different, however. One fiber has a polyether soft segment composed of poly(tetramethylene–oxide) with a prepolymer molecular weight of about 2000. The fiber denier is 1120 and the strain at break is approximately 500%. The second fiber has a copolyester soft segment of about 3500 molecular weight, which is synthesized from a mixture of ethylene glycol, butane diol, and adipic acid. This fiber has a denier of 650 and a 600% breaking strain.

METHODS

Power Cycles. Experimental thermodynamic cycles were obtained for the elastomers using an Instron Hydraulic Tensile Tester fitted with a specially designed quick-response environmental chamber. The experimental apparatus is shown schematically in Figure 1. A ramp strain program was used to cyclically deform the elastomer between a minimum (λ_{min}) and maximum (λ_{max}) elongation ($\lambda = L/L_0$) in a fixed amount of time. As a consequence of the fixed time interval (10 s), strain rates for extension and contraction varied from $\lambda = 0.2$ to $0.6 \, s^{-1}$. Previous experiments have shown that the mechanical response of these materials is insensitive to variations of four decades of strain rate.

The sample temperature was cycled between a low ($T_{LO} = 10°C$) and various high temperatures ($T_{HI} = 40°C, 60°C, 80°C, 100°C, 120°C$) by alternately forcing cold and hot dry air through the sample chamber at a flow rate of $1.5 \, L \cdot s^{-1}$. This produced a heating and cooling rate in the sample
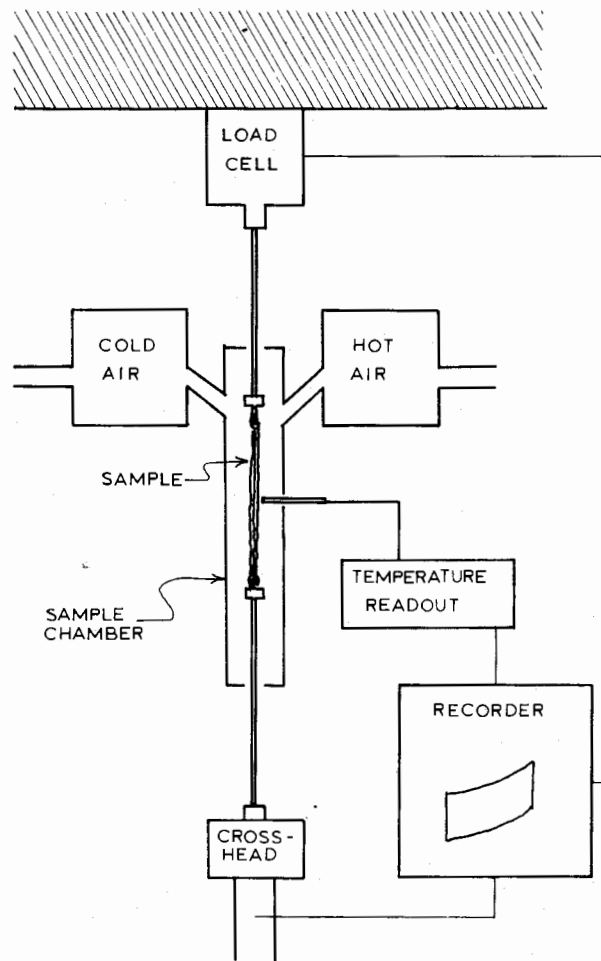

Fig. 1. Heat engine cycling apparatus.

of 200°C/min. Heating of incoming air was accomplished by using an in-line 1500-W resistance heater. Cold air was supplied through copper tubing heat exchange coils immersed in liquid nitrogen. Sample temperature was measured at the fiber surface using an Omega RTD platinum resistance probe whose thermal response was matched to that of the fiber. The cyclic strain and temperature program used to impart the thermodynamic cycle to the elastomer fibers is perhaps best illustrated schematically as in Figure 2.

The purpose of this strain–temperature program is to cycle the elastomer through the idealized thermodynamic cycle shown in Figure 3. The individual thermodynamic processes are:

1 → 2: The elastomer is deformed isothermally at T_{LO} from λ_{min} to λ_{max}, releasing heat Q_{12} to the low temperature reservoir. Work is done on the elastomer during this step.

2 → 3: The temperature is raised from T_{LO} to T_{HI} at λ_{max} adding heat Q_{23} to the elastomer. Since elastomers possess positive force vs. temperature coefficients in the extended state, the force is expected to increase at constant strain. No work is done during this step.

3 → 4: The elastomer is allowed to contract isothermally at T_{HI} from λ_{max} to λ_{min}, doing work in the process. An amount of heat, Q_{34}, is absorbed from the high temperature reservoir.

4 → 1: The temperature is lowered from T_{HI} to T_{LO} at λ_{min}, extracting an amount of heat Q_{41} from the sample. The force decreases on the elastomer due to cooling, but no work is done. The elastomer is thus returned to the initial state completing the cycle.

A direct graphical recording of the actual experimental cycle, as idealized above, was obtained by measuring force vs. displacement on a Hewlett-Packard x-y-y recorder. The work performed on or by the elastomer during the cycle is obtained as the area bounded by the closed curve 1–2–3–4–1 of Figure 3. Sample temperature was simultaneously measured on the third channel.
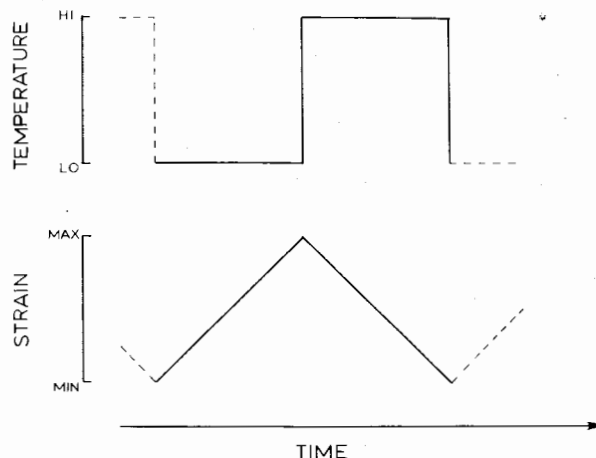

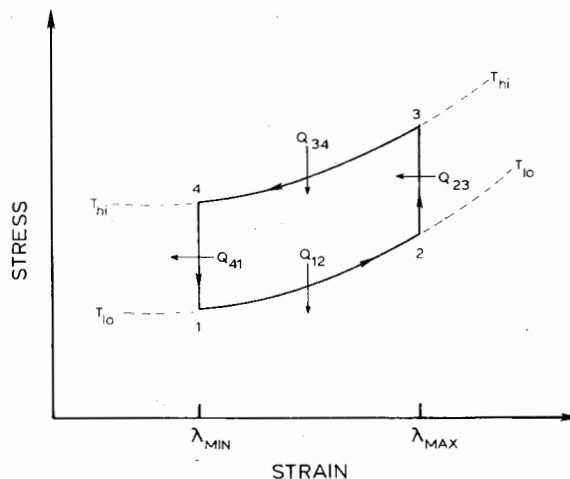Fig. 2. Strain–temperature program for heat engine cycles.

Fig. 3. Idealized heat engine cycle.

Separate fiber samples of approximately 70 mg were used for each strain perturbation after suitable equilibration at the maximum strain and temperature of the cycle. Thermodynamic cycles were performed until reproducible traces were obtained for those conditions of the cycle. This usually required five to seven preconditioning cycles.

Differential Scanning Calorimetry on Deformed Samples. Details of this method have been published.[19] Fiber samples are stretched to the desired elongation and wound onto small brass spools in the deformed state. The ends are then secured to prevent contraction of the sample while the experiment is conducted in a conventional Perkin-Elmer DSC II Differential Scanning Calorimeter.

Isothermal Deformation Calorimetry. An instrument was constructed based on the original design by Müller and Engelter[20] to simultaneously record the heat and work of the deformation process. The deformation calorimeter and measurement technique have been described.[21] Changes of internal energy in the sample during deformation are obtained as the difference between the heat and the work measured by the deformation calorimeter, as required by the first law of thermodynamics.

RESULTS

The mechanical work per cycle obtained from these elastomers during the previously described thermodynamic cycle was determined graphically as the area enclosed by the experimental curve. These areas, in units of force $\times$ displacement, were divided by the mass of the sample to yield values for the work per cycle per unit mass (J/g elastomer). Numerical values of the cycle work obtained for each particular set of independent experimental variables (e.g., λ_{min}, λ_{max}, T_{LO}, T_{HI}) are reported in Tables I and II for the polyether and polyester soft segment elastomers, respectively.

The sign convention used for this data is that positive cycle work corresponds to work which is done by the elastomer on the surroundings during a complete cyclic process. This means that more work was done by the

TABLE I
Polyether Soft Segment Elastomer

λ_{min}	λ_{max}	T_{LO}	T_{HI}	W_c	T_{HI}	W_c	T_{HI}	W_c	T_{HI}	W_c	T_{HI}	W_c
2.0	2.5	10	40	0.25	60	0.25	80	0.31	100	0.21	120	—
2.0	3.0	10	40	0.13	60	0.29	80	0.25	100	0.22	120	—
2.0	3.5	10	40	−0.26	60	−0.17	80	0.03	100	0.07	120	—
2.0	4.0	10	40	−1.00	60	−0.45	80	−0.15	100	−0.59	120	—
2.0	4.5	10	40	−1.94	60	−1.61	80	−1.5	100	−1.60	120	—
2.0	5.0	10	40	−2.45	60	−2.88	80	−3.07	100	−2.60	120	—
2.5	3.0	10	40	0.34	60	0.37	80	0.42	100	0.41	120	—
2.5	3.5	10	40	0.33	60	0.30	80	0.57	100	0.57	120	—
2.5	4.0	10	40	−0.20	60	−0.08	80	−0.08	100	0.36	120	0.40
2.5	4.5	10	40	−1.03	60	−0.56	80	−0.17	100	0	120	−0.21
2.5	5.0	10	40	−2.10	60	−1.40	80	−1.70	100	−0.47	120	−0.68
3.0	3.5	10	40	0.36	60	0.49	80	0.51	100	0.48	120	0.40
3.0	4.0	10	40	0.10	60	0.50	80	0.57	100	0.72	120	0.53
3.0	4.5	10	40	−0.16	60	0.12	80	0.40	100	0.68	120	−0.42
3.0	5.0	10	40	−0.92	60	−0.97	80	−1.01	100	0.27	120	0.18
3.5	4.0	10	40	0.37	60	0.55	80	0.62	100	0.51	120	0.43
3.5	4.5	10	40	0.14	60	0.48	80	0.76	100	0.81	120	0.62
3.5	5.0	10	40	−0.97	60	−0.54	80	−0.11	100	0.62	120	0.67
4.0	4.5	10	40	0.41	60	0.62	80	0.72	100	0.62	120	0.50
4.0	5.0	10	40	0.15	60	0.38	80	0.84	100	0.93	120	0.82
4.5	5.0	10	40	0.50	60	0.66	80	0.71	100	0.80	120	0.60

TABLE II
Polyester Soft Segment Elastomer

λ_{min}	λ_{max}	T_{LO}	T_{HI}	W_c	T_{HI}	W_c	T_{HI}	W_c	T_{HI}	W_c	T_{HI}	W_c
2.0	2.5	10	40	0.14	60	0.17	80	0.10	100	0.09	120	—
2.0	3.0	10	40	0.24	60	0.27	80	0.21	100	0.09	120	—
2.0	3.5	10	40	0.26	60	0.19	80	0.26	100	0.01	120	—
2.0	4.0	10	40	−0.06	60	0.16	80	−0.07	100	0.07	120	—
2.0	4.5	10	40	−0.90	60	0.16	80	0.23	100	−0.38	120	—
2.0	5.0	10	40	−0.51	60	−0.42	80	−0.19	100	−0.68	120	—
2.0	5.5	10	40	−2.50	60	−1.30	80	−0.80	100	−0.74	120	—
2.0	6.0	10	40	−2.81	60	−3.54	80	−1.33	100	—	120	—
2.5	3.0	10	40	0.25	60	0.21	80	0.23	100	0.12	120	—
2.5	3.5	10	40	0.38	60	0.38	80	0.30	100	0.26	120	—
2.5	4.0	10	40	0.34	60	0.38	80	0.53	100	0.31	120	—
2.5	4.5	10	40	0.21	60	0.35	80	0.34	100	0.18	120	−0.09
2.5	5.0	10	40	−0.16	60	0.03	80	0.27	100	0.08	120	−0.11
2.5	5.5	10	40	−2.00	60	−0.44	80	−0.06	100	−0.22	120	−0.50
2.5	6.0	10	40	−2.60	60	−1.65	80	−0.36	100	−0.43	120	—
3.0	3.5	10	40	0.28	60	0.26	80	0.28	100	0.24	120	—
3.0	4.0	10	40	0.39	60	0.45	80	0.35	100	0.37	120	0.13
3.0	4.5	10	40	0.21	60	0.68	80	0.63	100	0.27	120	0.20
3.0	5.0	10	40	0.11	60	0.29	80	0.68	100	0.55	120	0.13
3.0	5.5	10	40	−1.20	60	0.36	80	0.31	100	0.47	120	0.06
3.0	6.0	10	40	−2.34	60	−1.0	80	0.14	100	0.23	120	−0.07
3.5	4.0	10	40	0.28	60	0.35	80	0.32	100	0.27	120	0.24
3.5	4.5	10	40	0.39	60	0.60	80	0.64	100	0.32	120	0.24
3.5	5.0	10	40	0.29	60	0.70	80	0.73	100	0.51	120	0.45
3.5	5.5	10	40	−1.20	60	0.19	80	0.71	100	0.65	120	0.53
3.5	6.0	10	40	−2.30	60	−1.30	80	0.54	100	0.65	120	0.55
4.0	4.5	10	40	0.26	60	0.33	80	0.39	100	0.19	120	0.21
4.0	5.0	10	40	0.50	60	0.61	80	0.61	100	0.53	120	0.37
4.0	5.5	10	40	−0.66	60	0.42	80	0.62	100	0.72	120	0.55
4.0	6.0	10	40	−1.50	60	−0.71	80	0.72	100	0.98	120	0.81
4.5	5.0	10	40	0.30	60	0.47	80	0.42	100	0.34	120	0.24
4.5	5.5	10	40	−0.36	60	0.33	80	0.68	100	0.66	120	0.46
4.5	6.0	10	40	−1.10	60	−0.82	80	0.68	100	0.76	120	0.65
5.0	5.5	10	40	0.20	60	0.31	80	0.41	100	0.45	120	0.39
5.0	6.0	10	40	−0.21	60	0.34	80	0.61	100	0.70	120	0.61
5.5	6.0	10	40	0.04	60	0.32	80	0.48	100	0.49	120	0.36

elastomer during contraction at T_{HI} than was required to extend it at T_{LO}. Conversely, negative cycle work indicates that the surroundings (e.g., the Instron) have done work on the elastomer during a complete cycle. This is evidenced as requiring more work to extend the elastomer at T_{LO} than is obtained during the contraction at T_{HI}.

Some representative power cycle data are shown in Figures 4 and 5. The effect on the sign and magnitude of the cycle work caused by changing the perature difference (ΔT) between the hot and cold reservoirs at fixed displacement ($\Delta\lambda$), is illustrated in Figure 4. These data curves are for the polyester elastomer at $\lambda_{min} = 5.0$, $\lambda_{max} = 6.0$, and $T_{LO} = 10°C$, with T_{HI} ranging from 40°C to 100°C as indicated by the appropriate ΔT. Additional data is shown in Figure 5 for the polyether elastomer at fixed ΔT and variable displacement. In this series $\lambda_{min} = 3.0$ while $\lambda_{max} = 3.5$, 4.0, 4.5, and 5.0.

First scan DSC data are shown in Figures 6 and 7 for the polyether and polyester soft segment elastomers, respectively, which had been stretched at room temperature and constrained at various extension ratios. The endotherm above room temperature appearing at higher extensions in both elastomers has been identified with the melting of strain-induced crystallization (SIC) of the soft segments by wide-angle X-ray scattering. Although the soft segments of each elastomer are different, these data indicate some common features in their strain-crystallization behavior. In particular, it is observed that SIC melts over a broad temperature range for both soft segment polymers, and develops rather abruptly at strains of approximately one half of the breaking elongation. Once formed, the amount of SIC increases very little for successively higher strains, maintaining a relatively constant value of approximately 20%.

This is confirmed by deformation calorimetry, in which the heat (Q) and work (W) of loading were measured at room temperature in $\Delta\lambda = 0.5$ increments from $\lambda = 1$ to $\lambda = 5$ for the polyether soft segment elastomer. The measured ratio of the heat envolved to the work done on the elastomer (e.g., $\Delta Q/\Delta W$) for each incremental strain are plotted in Figure 8 vs. extension ratio. Ideal elastomers would be expected to yield a value of unity for this ratio, since in the absence of internal energy changes the heat
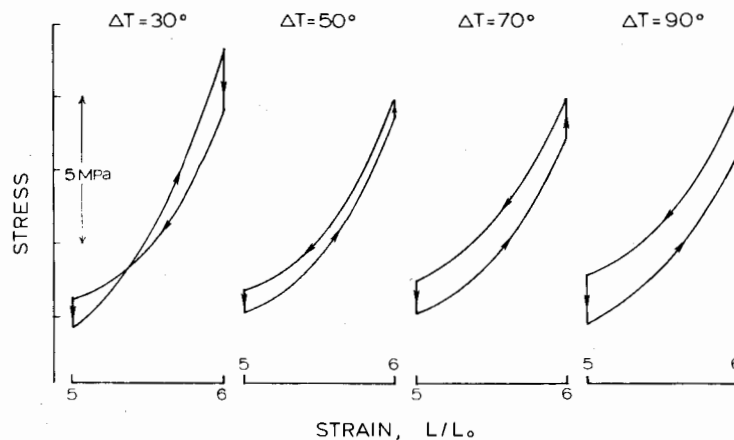

Fig. 4. Experimental power cycles for polyester elastomer, vertically shifted for clarity.
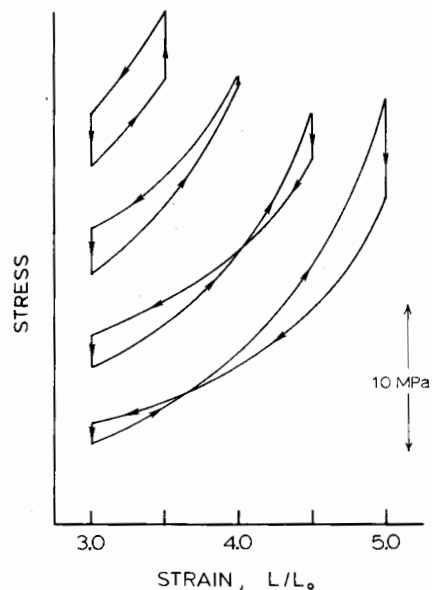
Fig. 5. Experimental power cycles for polyether elastomer, vertically shifted for clarity. $\Delta T = 50°C$.

should equal the work in the same units of energy. For this polyether soft segment elastomer, however, it is observed that the heat evolved during stretching can exceed the work done on the elastomer by a factor of 6. This excess heat of deformation has been observed in similar polyurethanes[22,23] and corresponds to the latent heat of fusion liberated by the soft segment strain induced crystallization as measured by stretch DSC.[21]

DISCUSSION

The practical value of thermodynamic cycle data for evaluating the performance of elastomers in rubber heat engine cycles is best illustrated by some sample calculations. From Table II the maximum mechanical energy produced for the polyester soft segment fiber occurs between a minimum
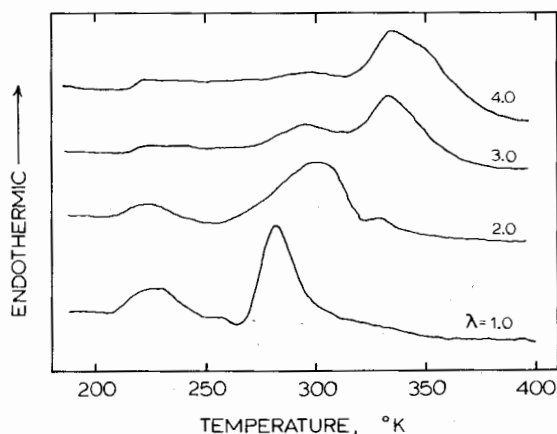
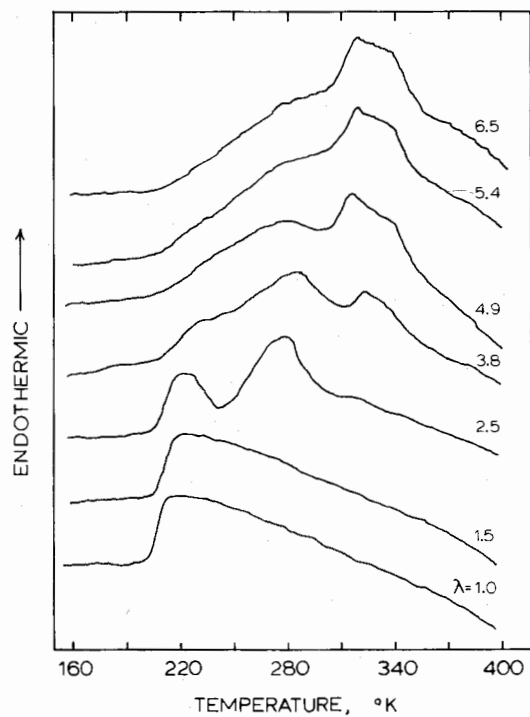Fig. 6. Differential scanning calorimetry data for stretched polyether elastomer.

Fig. 7.   Differential scanning calorimetry data for stretched polyester elastomer.
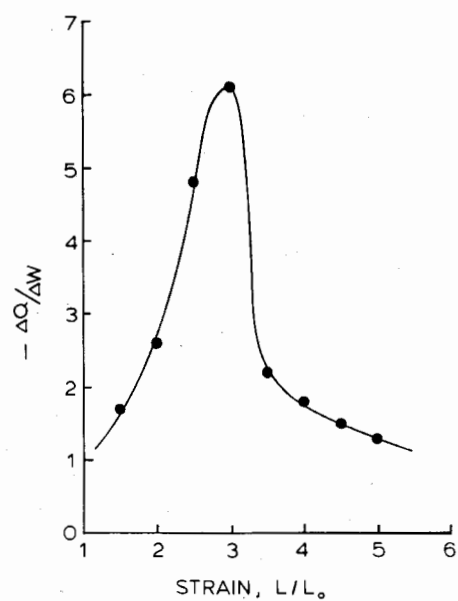

Fig. 8.   Ratio of incremental heat to work during stepwise extension of polyether elastomer.

extension of 4 and a maximum extension of 6 for $T_{HI} = 100°C$. Noting that this is ca. 1 J/g elastomer, a simple calculation may be made to determine the power of a rubber heat engine turning at 100 revolutions (cycles) per minute under these conditions. Assuming that this engine employs 1 kg of the polyester elastomer as the working substance, the power is calculated as

$$\text{power} = 1 \text{ J/g} \times 1000 \text{ g} \times 100 \text{ rpm} \times 1 \text{ min}/60 \text{ s}$$
$$= 1.7 \text{ kW}$$

This represents an upper bound since heat transfer and friction have been neglected. However, real engines have approached this limit.[16] The thermal efficiency (η) may be calculated for the isothermal cycle of Figure 3 by knowing the work per cycle (W_c) and the heat transferred to the material at the high temperature ($Q_{in} = Q_{23} + Q_{34}$).

Knowing that $W_c = 1$ J/g, and estimating Q_{in} from heat capacity and deformation calorimetry measurements,

$$\eta = \frac{W_c}{Q_{in}} = \frac{W_c}{Q_{23} + Q_{34}} = \frac{1 \text{ J/g}}{(1.6 \text{ J/g} \cdot \text{K} \times 100 \text{ K}) + (20 \text{ J/g})} = 0.7\% \quad (1)$$

This is approximately 3% of the theoretical efficiency of an engine operating between these temperatures. A more realistic cycle for an engine operating at high speed would be a cycle in which the mechanical processes (e.g., $1 \rightarrow 2$ and $3 \rightarrow 4$) are conducted adiabatically. In this case the measured thermal efficiency exceeds 3% of theoretical, although the work per cycle would necessarily decrease as the elastomer temperature approaches the source and sink temperatures due to adiabatic heating and cooling.

The importance of obtaining experimental thermodynamic cycle data becomes evident when a comparison is made to theoretical predictions obtained from the ideal rubber equation of state. Following the derivation of Ref. 5, the work per cycle (W_c) per unit volume for an ideal elastomer may be obtained from the thermomechanical equation of state as

$$W_c = \oint \sigma \, d\lambda \quad (2)$$

$$= \oint \frac{G_0 T}{T_0} \left(\lambda - \frac{1}{\lambda^2} \right) d\lambda \quad (3)$$

$$\simeq \frac{G_0}{2} \left[\frac{T_{HI} - T_{L0}}{T_0} \right] (\lambda_{max}^2 - \lambda_{min}^2) \quad (4)$$

where eq. (4) is approximately valid for $\lambda \geq 2$. In these equations, σ is the stress on the elastomer, and G_0 is the small strain shear modulus at T_0. While this equation predicts that mechanical energy is produced in a heat engine cycle at all strains and temperature differentials, the experimental data indicate that, for these elastomers, this is not the case. In particular, it is observed that, at large strain perturbation cycles, mechanical losses

occur which seem to be temperature-dependent. Conversely, in cycles where the strain perturbations are small, these elastomers produce positive mechanical work at all of the high temperatures tested for the cycle.

These observations are consistent with the results of numerous investigations connecting strain-induced crystallization (SIC) to the hysteresis behavior of elastomers in thermodynamic stress–strain cycles.[3,22,24,25] Specifically it is the changes of SIC during isothermal stretching and contraction which lead to the mechanical losses. Minimal mechanical losses are observed when SIC is unchanging[22] or is completely suppressed by cycling above the melting temperature of the crystallites.[24,25]

In the light of the above considerations, it is thought that the positive work cycles which occur at small strain perturbations may reflect reversible entropic elastomer behavior, since under these conditions losses associated with changing SIC during deformation are avoided. The temperature-independent effect of SIC in this context is the purely mechanical reinforcement of the high melting crystallites, which act as physical crosslinks, and may increase the elastic modulus by a factor of 100.[15]

The effect of increased modulus on the available work per cycle is revealed by eq. (4). For the experimental cycles of this study, in which the temperature of the elastomer is changed at fixed length, the following relationship is also applicable:

$$\left(\frac{\partial f}{\partial T}\right)_L = -\left(\frac{\partial f}{\partial L}\right)_T \left(\frac{\partial L}{\partial T}\right)_f \tag{5}$$

Multiplication by L_0/L_0 yields

$$\left(\frac{\partial f}{\partial T}\right)_L = -E\alpha \tag{6}$$

where the change in force (f) with temperature (T) at constant length (L) is seen to be proportional to the negative product of the tensile modulus (E) and the linear thermal expansion coefficient $(\alpha \equiv 1/L_0)dL/dT)$. For an incompressible material, $E = 3G_0$ of eq. (4). While E is always positive, α may be positive or negative. For stretched elastomers, α is negative, indicating that the force in a strained elastomer held at constant length would be expected to rise with temperature. This describes the processes $2 \rightarrow 3$ and $4 \rightarrow 1$ of Figure 3. The reinforcing effect of SIC, evidenced as an increase in the modulus, is seen to be directly related to the difference between the work performed on or by an elastomer in a cyclic thermodynamic process in which no phase changes occur during deformation. The moduli of these elastomers are also increased (relative to chemically crosslinked analogs), by the presence of hard segment domains.[26]

The negative or dissipative power cycles obtained at low temperature differentials and large strain perturbations reflect the large hysteresis losses routinely observed in these elastomers during room temperature stress–strain cycles. This is a natural consequence of the nonequilibrium amor-

phous–crystalline phase transformation of the soft segments.[27,28] Inhomogeneous stress distributions which result from crystallization during loading tend to increase the work of deformation in accord with free energy criteria for a nonequilibrium mechanical process. The instantaneous stress relaxation following loading to large strains (Figures 4 and 5) is an entropy driven approach to mechanical and phase equilibrium which results in a more homogeneous stress distribution and a lower free energy for the material.[29] Consequently, the elastomer is able to do less work on unloading and dissipative cycles are observed.

The transition from negative to positive power cycles at large strains with increasing T_{HI} is a result of the reduced tendency of these elastomers to strain crystallize after conditioning at high strains and temperatures. The reason for this is softening of the materials due to the disruption of the hard segment domains under these conditions, which results in a lower modulus material.[30] As a result of thermal softening, stresses sufficient to induce crystallization are not achieved during the high source temperature cycles and quasi-ideal (positive) power cycles are obtained.

PILOT SCALE OPERATION

While the previous thermodynamic analysis indicates a viable route to the utilization of polymers in energy conversion, it remains to demonstrate that these concepts may be successfully applied to a real world process. To this end we have built and tested a number of rubber heat engines in our laboratory which utilize the thermodynamic cycles presented earlier. The third generation engine in use today is shown in Figure 9.
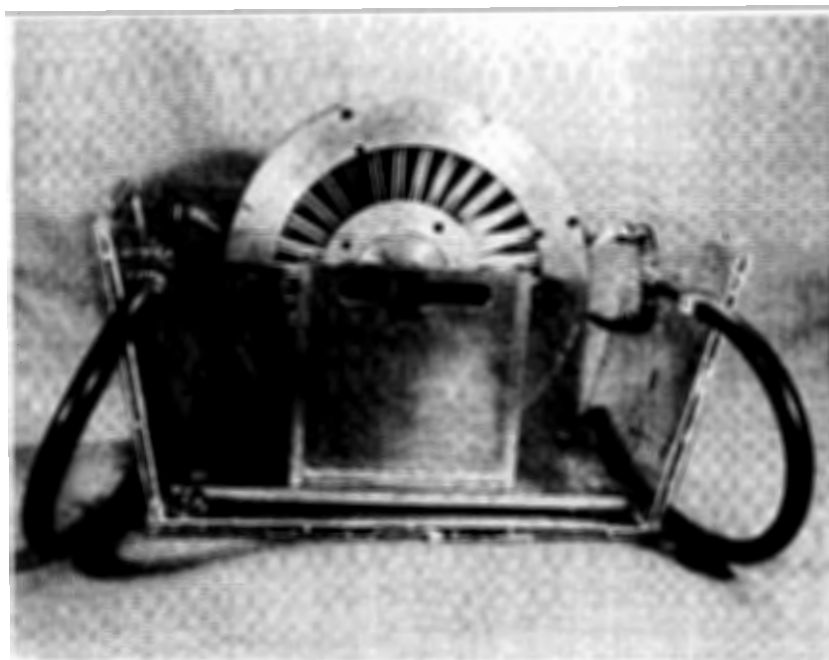

Fig. 9. Pilot scale rubber heat engine.

The engine operates by directing a stream of cold water on the low stretch side of the engine while applying a hot water stream to the high stretch side, 180° in opposition. The resulting torque couple causes rotation of the rubber element/hub assembly such that during steady state operation the rubber elements are continuously cycled between the opposing hot and cold water streams and high and low stretch. For each engine revolution the elastomer traverses a complete thermodynamic cycle.

This and similar engines have been operated continuously for 48 h and intermittently over a period of 3 years using the same elastomeric fiber elements. Although natural rubbers are known to be slowly degraded by environmental stresses, the synthetic polyurethane elastomers used in this study have shown excellent long-term stability with respect to repeated exposure to light and hot and cold water during engine operation.

Measurements of the power produced by the rubber heat engine have been made for various conditions of strain and temperature by direct coupling of the drive shaft to a torque-measuring dynamometer. In Figure 10 is shown a plot of such data for engine power (W) vs. engine speed (rpm) at various temperature differences (ΔT) for an engine using about 100 g of the polyether elastomer. These data were obtained at $\lambda_{min} = 2.5$ and $\lambda_{max} = 3.0$.

Maxima in the power curves correspond to the thermal response time ($\sim$ 100 ms) of the elastomer fiber elements, indicating that higher speeds may be obtained by increasing the rate of heat transfer to the fibers. Plots such as Figure 11 show that the peak power obtained from Figure 10 is proportional to ΔT above a certain small value, this corresponding to the threshold for negative power cycles of the previous section.

The observed linear relationship between rubber heat engine power maxima and increasing temperature difference suggest quasi-ideal rubber behavior which is not evidenced in the power cycle data. This may be due to the fact that, in contrast to the experimental cycles, the elastomers working in the rubber engine at high speeds never come to thermal equilibrium with the source and sink. Instead, these elastomer fibers undergo small
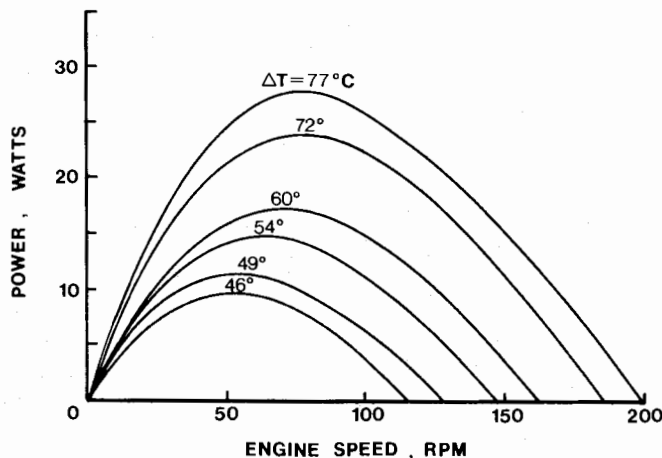

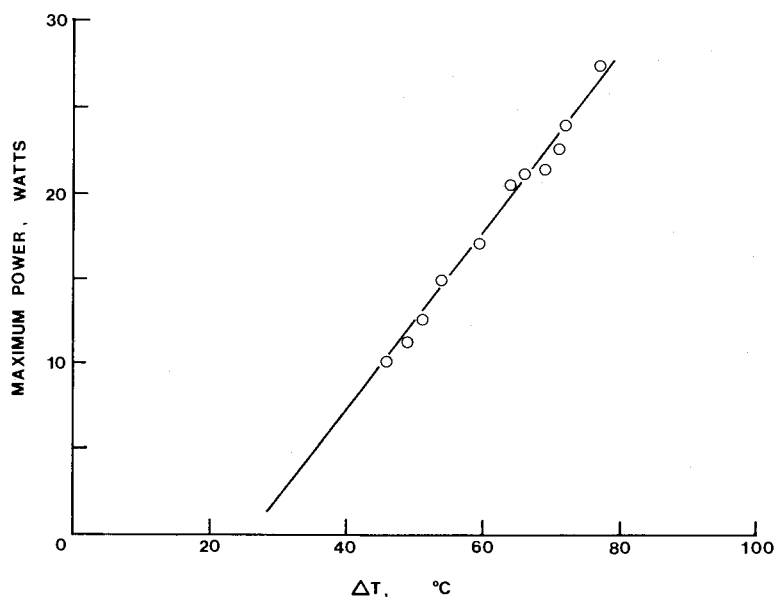Fig. 10. Rubber heat engine power vs. engine speed.

Fig. 11. Maximum rubber heat engine power vs. temperature difference between hot and cold water.

thermal fluctuations about some intermediate temperature which, combined with the small strain perturbations, reduce the effects of nonideal phenomenon such as strain- and thermally induced microstructural changes.

CONCLUSIONS

In this paper we have investigated the role of strain-induced crystallization on the heat engine cycles of two synthetic elastomers. It was observed that power cycles obtained under conditions which promote strain-induced crystallization during the mechanical portions of the cycle do not yield useful work. This is not due to the phase transformation itself, which if conducted reversibly should increase the available work per cycle.[7] Instead, it is the inherent nonequilibrium nature of the process which is responsible for the lost work.

The positive cycle work available from these elastomers under optimum conditions ($W_c \simeq 1$ J/g) reflects mainly entropic behavior, but exceeds natural rubber by a factor of 10. This is due to the higher modulus of these materials resulting from the domain structure, and possibly some strain-induced crystallinity which persists above the source temperature at large strains and small strain perturbations.

Although the conversion efficiency of heat to work is small, it is typical of engines utilizing low grade heat. Conversely, these materials functioning in reversed cycles for heat pumping would be very efficient, especially in view of the large amount of heat transported by strain-induced crystallization. The coefficient of performance (ω) for such a heat pump is given by $\omega = Q_{out}/W_{in}$, where W_{in} is the work done on the substance during one complete cycle. The maximum value of $\Delta Q/\Delta W = -6$ obtained for loading

of the elastomer in Figure 8 corresponds to $\omega = 13$, since 46% of the work of loading is lost during a small perturbation cycle at that strain. This is approximately twice the performance of existing commercial units.

References

1. W. S. Ginell, J. L. McNichols, and J. S. Cory, presentation at ASME Intersoc. Conf. on Environmental Systems, San Diego, Calif., July 10–13, 1978.

2. W. B. Wiegand, *Trans. Inst. Rubber Ind.*, **1**, 46 (1925).

3. W. B. Wiegand and J. W. Snyder, *I.R.I. Trans.*, **10**, 234 (1934).

4. C. L. Strong, *Sci. Am.*, **224**(4), 118–22 (1971).

5. R. J. Farris, *Polym. Eng. Sci.*, **17**(10), 737 (1977).

6. L. Mandelkern, D. E. Roberts, A. F. Diorio, and A. S. Posner, *J. Am. Chem. Soc.*, **81**, 4148 (1959).

7. L. Mandelkern, *Crystallization of Polymers*, McGraw-Hill, New York, 1964, Chap. 7.

8. Patent issued to NASA; reported in *Mech. Eng.* (Apr), 47 (1971).

9. I. Z. Steinberg, A. Oplatka, and A. F. Katchalsky, *Nature*, **210**, 568 (1966).

10. W. Kuhn and M. Thuerkauf, *Kolloid-Z.*, **184**, 114 (1962).

11. W. Kuhn, *Makromol. Chem.*, **35**, 200 (1960).

12. M. N. Sarbolouki and R. F. Fedors, *J. Polym. Sci., Polym. Lett. Ed.*, **17**, 629 (1979).

13. G. Smets, J. Braeken, and M. Irie, *Pure Appl. Chem.*, **50**(8), 845 (1978).

14. A. Katchalsky and P. F. Curran, *Nonequilibrium Thermodynamics in Biophysics*, Harvard University Press, Cambridge, Mass., 1965, Chap. 3.

15. L. R. G. Treloar, *The Physics of Rubber Elasticity*, Clarendon, P, Oxford, 1958, Chap. 2.

16. R. J. Farris and R. E. Lyon, Proceedings of NSF Workshop on Substituting Non-Metallic Materials for Vulnerable Minerals, Washington, D.C., June 27, 1983.

17. E. M. Hicks, A. J. Ultee, and J. Drougas, *Science*, **147**(3656), 373–379 (1965).

18. R. A. Gregg, *Encyclopedia of Chemical Technology*, Wiley, New York, 1969, Vol. 18, pp. 614–633.

19. R. E. Lyon, R. J. Farris, and W. J. MacKnight, *J. Polym. Sci., Polym. Lett. Ed.*, **21**(5), 323 (1983).

20. F. H. Muller and A. Engelter, *Rheol. Acta*, 1, 39 (1958).

21. R. J. Farris and R. E. Lyon, Proceedings of the Fourth Cleveland Symposium on Macromolecules: Irreversible Deformation of Polymers, June 13, 1983.

22. L. Morbitzer and H. Hespe, *J. Appl. Polym. Sci.*, **16**, 2697–2708 (1972).

23. L. Morbitzer and R. Bonart, *Kolloid Z. Z. Polym.*, **232**(2), 764 (1969).

24. G. L. Clark, M. Kabler, E. Blaker, and J. M. Ball, *Rubber Chem. Tech.*, **14**(1), 27–34 (1941).

25. L. Airamo, F. deCandia, and V. Vittoria, *Polymer*, **19**, 731 (1978).

26. C. B. Wang and S. L. Cooper, *Macromolecules*, **16**, 775 (1983).

27. P. J. Flory, *J. Chem. Phys.*, **15**(6), 397 (1947).

28. T. Alfrey, *Mechanical Behavior of High Polymers*, Wiley-Interscience New York, 1948, Chap. B.

29. R. Bonart, *J. Macromol. Sci. Phys.*, **B2**(1), 115 (1968).

30. D. X. Wang, R. E. Lyon, and R. J. Farris, *J. Macromol. Sci.*, to appear.